UHasselt Computational Mathematics Preprint Series

Hysteresis and Horizontal Redistribution in Porous Media

Hans van Duijn and Koondanibha Mitra

UHasselt Computational Mathematics Preprint
Nr. UP-17-05

July 5, 2017

Hysteresis and Horizontal Redistribution in Porous Media

C.J. van Duijn [1,2] *and* K. Mitra*[3,4]

[1] *Eindhoven University of Technology, Department of Mechanical Engineering*
[2] *University of Utrecht, Department of Earth Sciences*
[3] *Eindhoven University of Technology, Department of Mathematics and Computer Science*
[4] *Hasselt University, Faculty of Sciences*

July 4, 2017

Abstract

It is well known that multi-phase flow in porous media exhibits hysteretic behaviour. This is caused by different fluid-fluid behaviour if the flux reverses. For instance, in unsaturated ground water flow the process of imbibition and drainage behave differently. In this paper we study a new model for hysteresis that extends the current play-type hysteresis model in which the scanning curves between drainage and imbibition are vertical. In our approach the scanning curves are non-vertical and can be constructed to approximate experimentally observed scanning curves. Furthermore our approach does not require any book-keeping when the flux reverses at some point in space. Specifically, we consider the problem of horizontal redistribution to illustrate the strength of the new model. We show that all cases of redistribution can be handled, including the unconventional flow cases. Our analysis uses a self-similar transformation of the equations. We also present a numerical approach (L-scheme) for the partial differential equations in a finite domain to recover all redistribution cases of the infinite column provided time is not too large.

1 Introduction

In this paper we consider the flow of two immiscible and incompressible fluids through a homogeneous and isotropic porous medium. It is assumed that the pores of the medium are fully occupied by these fluids. One fluid is the wetting phase and the other one is

*Corresponding author: email: k.mitra@tue.nl

the non-wetting phase. They are denoted by the subscripts w and n. We disregard the influence of gravity, as we are interested in a horizontal physical system. Further we assume that there are no internal sinks or sources. The corresponding (i.e. macroscopic) equations are well-known [1, 5, 9] and in dimensionless form they read:

$$\partial_t S_i + \nabla \cdot \vec{F}_i = 0, \quad \vec{F}_i = -k_i(S_i)\nabla P_i \qquad \text{for } i = n, w; \tag{1.1}$$

$$S_n + S_w = 1, \qquad S_n, S_w \geq 0. \tag{1.2}$$

In (1.1), S_i, P_i and $\vec{F}_i$ denote saturation (assumed to be scaled such that $0 \leq S_i \leq 1$), pressure and volumetric flux of phase i, and k_i is the relative permeability of the porous medium with respect to phase i. If the system contains water as the wetting phase and air as the non-weeting phase, then it is generally assumed that $P_n = P_{air}$ is constant. The equations (1.1) reduce to Richards equation which is the standard equation that models unsaturated flow in porous domains [1, 5, 9]:

$$\partial_t S_w + \nabla \cdot \vec{F}_w = 0, \quad \vec{F}_w = -k_w(S_w)\nabla P_w \qquad \text{with } 0 \leq S_w \leq 1. \tag{1.3}$$

In general, the closure relation between P and S is given in form of an algebraic relationship determined from experiments:

$$P_n - P_w = P_c(S_w), \tag{1.4}$$

where $P_c : (0, 1] \to \mathbf{R}$ is the capillary pressure. There is a vast amount of literature available on the capillary pressure and its interpretation [1, 5, 9]. For properties and closed-form relations we refer to the well-known references [4, 25].

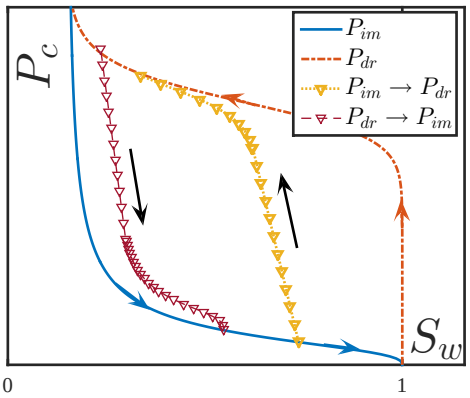

(a) Schematic diagram of primary infiltration, drainage and scanning curves [27].

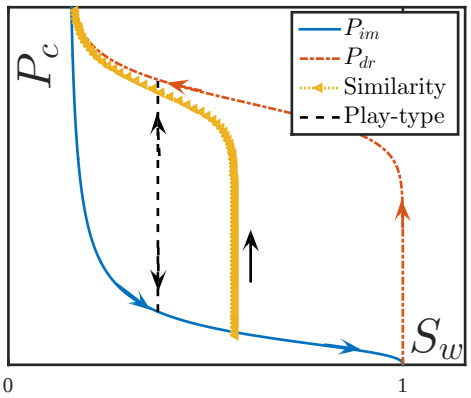

(b) Schematic diagram of scanning curves for playtype hysteresis and similarity models [2, 12].

Figure 1: P_c-S_w relationships from experiments and existing models

It is known that multiphase flow in porous media displays hysteretic effects [20]. The capillary pressure-saturation relationship (henceforth called P_c-S_w relationship) traces one path while going through an infiltration/imbibition/wetting process and another path while going through a drainage/drying process. This effect can be incorporated into the classical model by replacing $P_c(S_w)$ function in (1.4) by two different functions: $P_{im}(S_w)$ for infiltration and $P_{dr}(S_w)$ for drainage. This works quite well if the porous medium is going through only an infiltration or a drainage process. But if there is a switch between the two, then the P_c-S_w curves span the region between the P_{im} and P_{dr} curves in form of scanning curves [11]. Typical behaviour is shown in Figure 1. Some of the most common models for porous media hysteresis are:

1.1 Similarity models

The main idea behind this class of models is to express the scanning curves by a closed-form relationship that allows the scanning curve to be similar in shape to the imbibition or drainage curves. With the similarity hypothesis, Philip [16] was able to get reasonable approximations for scanning curves. Later models such as the Mualem model [12] and the Lenhard-Parker model [14] were developed using similar concepts. The scanning curves obtained in this way are close to the experimental scanning curves. Moreover, this class of models can describe "secondary hysteresis". This refers to the phenomenon that the scanning curve through a point, switching from imbibition to drainage, is different from scanning curve through the same point switching from drainage to imbibition. All other models discussed in this paper do not include this secondary behaviour, because for those models a intermediate point can move back and forth on the same scanning curve. Similarity models can also be used to explain many cases of the horizontal redistribution problem [8], which is an important benchmark problem for porous flows.

However similarity models are not straightforward to apply because in these models the saturation at a point is a function of all previous reversal points (when it switches from infiltration to drainage or vice versa). The closed-form expressions of the scanning curves actually take in these reversal points as parameters. The order at which the processes (imbibition/drainage) have gone through plays also a vital role. This leads to book-keeping for each point in space, making the models difficult to handle in practice and in any numerical or analytical approach.

1.2 Playtype hysteresis

In this approach one models scanning curves as vertical lines between P_{im} and P_{dr} [2, 22, 26]. To close relation (1.1) one proposes the form:

$$P_n - P_w := P_c\left(S_w, \partial_t S_w\right) \in P^+(S_w) - P^-(S_w) \cdot \operatorname{sign}\left(\partial_t S_w\right), \tag{1.5}$$

where sign(ζ) is the multivalued signum graph,

$$\operatorname{sign}(\zeta) = \begin{cases} 1 & \text{for } \zeta > 0 \\ [-1,1] & \text{for } \zeta = 0 \\ -1 & \text{for } \zeta < 0, \end{cases} \tag{1.6}$$

and where P^+, P^- are defined by:

$$P^+ := \frac{1}{2}\left(P_{dr} + P_{im}\right), \quad P^- := \frac{1}{2}\left(P_{dr} - P_{im}\right). \tag{1.7}$$

This model implies that if $\partial_t S_w > 0$, then $P_n - P_w = P^+(S_w) - P^-(S_w) = P_{im}(S_w)$, and if $\partial_t S_w < 0$, then $P_n - P_w = P^+(S_w) + P^-(S_w) = P_{dr}(S_w)$. If $P_{im}(S_w) < P_n - P_w < P_{dr}(S_w)$, then $\partial_t S_w = 0$.

The model, including this form of hysteresis, is well posed [10] and is physically justifiable by pore-scale [21] or thermodynamic [2] arguments. Although this model has the advantage of being simple and local in time (no information on the history of a point is required) the resulting vertical scanning curves do not really resemble the ones from experiments. Moreover, as we show later, playtype hysteresis model cannot describe all cases of horizontal redistribution for many known cases.

1.3 Interfacial area model

Pore-scale simulations have shown that interfacial areas plays an important role in the P_c-S_w relationship. Motivated by this, a model was proposed in [6, 7, 13] based on thermodynamic considerations. The main idea is to introduce the volumetric interfacial area (a_{wn}) as a new variable, in addition to saturation and pressure, and to assume that a_{wn} is a unique function of saturation and pressure:

$$a_{wn} = a_{wn}(S_w, P_n - P_w). \tag{1.8}$$

A transport equations for a_{wn} was proposed leading to a new formulation for multiphase flow, including hysteretic behaviour. The model was analyzed in [18] for horizontal redistribution. There it was shown that for any fixed point x_0 in space, there exists a unique P_c-S_w curve which satisfies

$$\frac{dP_c}{dS}(S_w) = g(P_c, S_w), \qquad \text{with } P_c(S_w(x_0, 0)) = P_c(x_0, 0), \tag{1.9}$$

where g is a given smooth function of P_c and S_w. Thus if $S_w(x, 0)$ and $P_c(x, 0)$ have only two values, as they do for horizontal redistribution, two P_c-S_w curves arise. Clearly for general initial conditions, infinitely many P_c-S_w curves may arise. However the concept of

primary imbibition and drainage is not described by this model. Hysteresis, in the sense of switching between two curves at a fixed x_0, could only be included by introducing rate dependent terms in the coefficients [27, p. 67].

The purpose of this paper is to introduce a hysteresis model that is based on the play-type approach, having primary drainage/imbibition curves and in between non-vertical scanning curves. These scanning curves can be chosen in such a way that they are close to experimental data. This model is presented and discussed in Section 2. In Section 3 the equations and conditions for (horizontal) redistribution are given and in Section 4 self-similar solutions are discussed describing all possible redistribution cases using the new model. Then, in Section 5 a numerical scheme (L-scheme) for the partial differential equation is presented and computational results are compared with the redistribution cases. Conclusion are given in Section 6.

2 Extended playtype hysteresis model

In this section we will introduce the extended playtype hysteresis model, discuss its background and some of its properties. Let u denote the capillary pressure, i.e.

$$u := P_n - P_w. \tag{2.1}$$

We extend the playtype hysteresis by introducing non-vertical scanning curves which become vertical near the end points $S_w = 0$ and $S_w = 1$. To this end we replace $\partial_t S_w$ in the sign function by $\partial_t(H(S_w)+u)$, where $H : (0,1) \to (0,\infty)$ is a function chosen in such a way that the corresponding scanning curves have the desired properties. Thus instead of (1.5) we propose

$$u \in P^+(S_w) - P^-(S_w) \cdot \operatorname{sign}(\partial_t H(S_w) + \partial_t u), \tag{2.2}$$

where $P^{\pm}(S_w)$ and $\operatorname{sign}(\cdot)$ are defined as in (1.7) and (1.6), respectively. To better understand what relation (2.2) implies, let us introduce the following sets:

Definition 1 *In the (S_w, u) plane we consider the sets*

$$\begin{aligned}
\mathcal{H} &:= \{(S_w,u) : S_w \in (0,1], P_{im}(S_w) < u < P_{dr}(S_w)\},\\
\partial\mathcal{H}^{dr} &:= \{(S_w,u) : S_w \in (0,1], u = P_{dr}(S_w)\},\\
\partial\mathcal{H}^{im} &:= \{(S_w,u) : S_w \in (0,1], u = P_{im}(S_w)\}.
\end{aligned}$$

In these definitions we avoid $S_w = 0$, as $P_{im}(S_w)$ and $P_{dr}(S_w)$ become singular at that point.

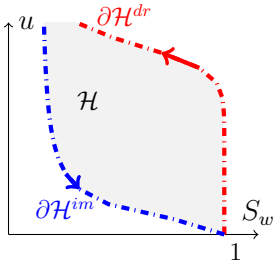

Figure 2: Sets in (S_w, u) plane according to Definition 1.

If $(S,u) \in \mathcal{H}$, then by (1.7)

$$-1 = \frac{P^+(S_w) - P_{dr}(S_w)}{P^-(S_w)} < \frac{P^+(S_w) - u}{P^-(S_w)} < \frac{P^+(S_w) - P_{im}(S_w)}{P^-(S_w)} = 1.$$

Hence from (2.2)

$$-1 < \text{sign}(\partial_t H(S_w) + \partial_t u) < 1.$$

Definition (1.6) of sign$(\cdot)$ then gives

$$\partial_t H(S_w) + \partial_t u = 0. \tag{2.3}$$

This means that we have

$$\frac{du}{dS_w} = -\frac{dH}{dS_w}(S_w) \text{ for } (S_w,u) \in \mathcal{H}, \tag{2.4}$$

implying scanning curves with slope $-\frac{dH}{dS_w}(S_w)$. Note that a point can move back and forth along the same scanning curve, see also Figure 4.

If $(S,u) \in \partial\mathcal{H}^{im}$ then,

$$\frac{P^+(S_w) - u}{P^-(S_w)} = \frac{P^+(S_w) - P_{im}(S_w)}{P^-(S_w)} = 1,$$

and hence $\text{sign}(\partial_t H(S_w) + \partial_t u) = 1$ implying

$$\partial_t H(S_w) + \partial_t P_{im}(S_w) = \left(\frac{dH}{dS_w} + \frac{dP_{im}}{dS_w}\right)\partial_t S_w \geq 0.$$

Thus if $\frac{dH}{dS_w} > -\frac{dP_{im}}{dS_w}$ we have

$$\partial_t S_w \geq 0 \text{ for } (S_w,u) \in \partial\mathcal{H}^{im}. \tag{2.5}$$

Similarly if $\frac{dH}{dS_w} > -\frac{dP_{dr}}{dS_w}$, then

$$\partial_t S_w \leq 0 \text{ for } (S_w,u) \in \partial\mathcal{H}^{dr}. \tag{2.6}$$

Now choosing H such that for each $0 < S_w \leq 1$

$$\frac{dH}{dS_w}(S_w) \geq \max\left\{-\frac{dP_{im}}{dS_w}(S_w), -\frac{dP_{dr}}{dS_w}(S_w)\right\}, \tag{2.7}$$

both the lower bound conditions are satisfied and so are inequalities (2.5) and (2.6). Moreover, condition (2.7) ensures that scanning curves originating from arbitrary points on $\partial\mathcal{H}^{im}$ or $\partial\mathcal{H}^{dr}$ remain in $\mathcal{H}$.

The question arises how to choose and construct a function H that gives scanning curves close to experimental data and satisfies (2.7) for mathematical consistency. We present a construction that is based on the experiment of Morrow and Harris [11]. Their results for drainage and imbibition are shown in Figure 3.

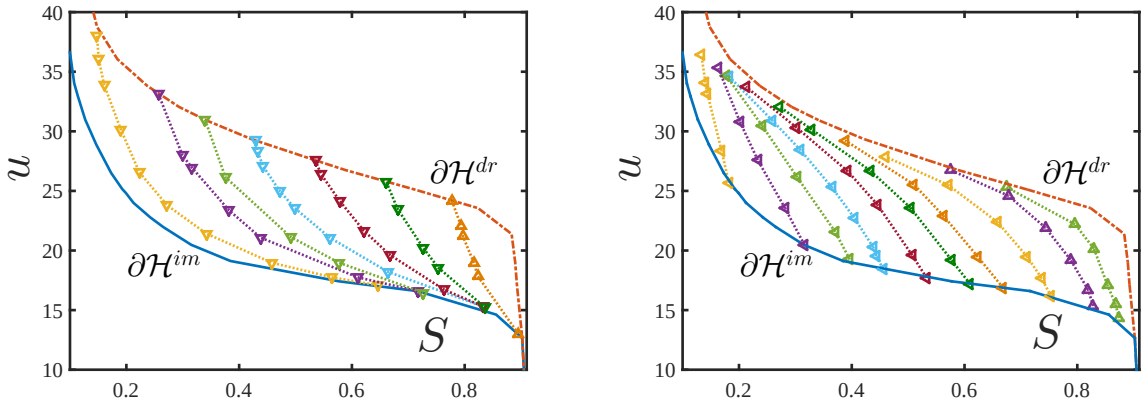

(a) (b)

Figure 3: Scanning curves: (a) experimental drainage (b) experimental imbibition (both after Morrow and Harris [11]).

Here the variables are as in [11]: the saturation is unscaled ($0 < S_{wr} < S_w < 1 - S_{ar}$) and the pressure (suction) is in cm of water. In the construction of H we use the same variables to get a meaningful comparison. We propose for H the form:

$$H(S_w) = \alpha(S_w) \int_{S_{\text{ref}}}^{S_w} \max\left\{ -\frac{dP_{im}}{dS_w}(S_w), -\frac{dP_{dr}}{dS_w}(S_w) \right\} dS, \tag{2.8}$$

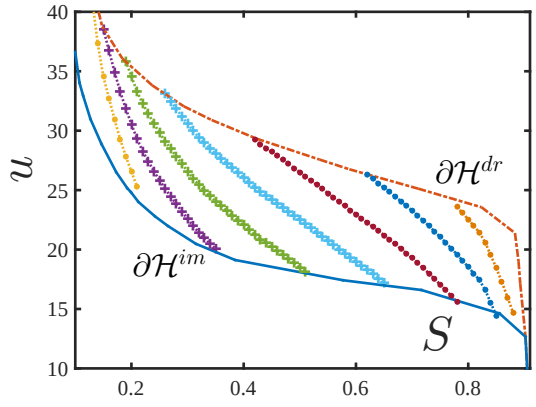

Figure 4: Scanning curves based on (2.8) and (2.9).

for $S_w > S_{\text{ref}}$, where S_{ref} is chosen close to S_{wr} (in fact $P_{im}(S_{\text{ref}}) = 35$) and P_{im} and P_{dr} are taken from the experiment. Clearly if $\alpha(S_w) \geq 1$ and $\frac{d\alpha}{dS_w}(S_w) \geq 0$, then (2.7) is satisfied. With trial and error we found that

$$\alpha(S_w) = 2\left(1 + \frac{1}{5}S_w^5\right), \tag{2.9}$$

gives a good approximation to both drainage and imbibition. The scanning curves shown in Figure 4 result from $u = \text{constant} - H(S_w)$, where the constant is defined by the intersection point with $\partial\mathcal{H}^{im}$ or $\partial\mathcal{H}^{dr}$.

The H obtained this way is a close match to the experiments. Having explicit expressions for P_{im} and P_{dr}, for instance the van Genuchten expressions, would result in a (semi) explicit expression for H.

Remark 1 *For simplicity one could consider* $\frac{dH}{dS_w}(S_w) := \frac{1}{\delta}$ *(is constant) for some* $\delta > 0$. *Then the scanning curves are described by the straight lines:*

$$\frac{du}{dS_w} = -\frac{1}{\delta}. \tag{2.10}$$

By the same argument as above, one would need for each $0 < S_w \leq 1$

$$\frac{1}{\delta} \geq \max\left\{-\frac{dP_{im}}{dS_w}(S_w), -\frac{dP_{dr}}{dS_w}(S_w)\right\}, \tag{2.11}$$

to ensure inequality (2.7). *However this would unrealistically restrict the range of saturations for which the scanning curves remain in* $\mathcal{H}$.

Beliave and Hassanizadeh [2] were the first to derive the extended playtype hysteresis closure relationship. Using thermodynamical arguments they obtained an expression in the inverse form of (2.2): see [2, eq. 35]. In our notation it translates into:

$$u \in P^+(S_w) - P^-(S_w) \cdot \operatorname{sign}\left[\left(1 - C\frac{dP_0^c}{dS_w}(S_w)\right)\partial_t S_w + C\partial_t u\right], \tag{2.12}$$

where $C > 0$ is a constant and P_0^c is a reference curve between P_{im} and P_{dr} that intersects all scanning curves. For example P_0^c could be P^+. The authors argued, using experimental data, that the term $CP_0^{c'}(S_w)$ has roughly 10% contribution in expression (2.12). Also they pointed out that $C \to 0$ corresponds to the playtype hysteresis model. As $C^{-1}(1 - C\frac{dP_0^c}{dS_w}(S_w)) > 0$ for each $0 < S_w \leq 1$, one could write,

$$\frac{dH}{dS_w}(S_w) := C^{-1} - \frac{dP_0^c}{dS_w}(S_w). \tag{2.13}$$

to put (2.12) in the form of (2.2). Note however that the reference pressure P_0^c does not necessarily satisfy condition (2.7).

Extension of playtype hysteresis model by inclusion of non-vertical scanning curves has been hypothesized also in context of numerical analysis. For example, in [3], authors use non-vertical approximations to vertical scanning curves as the original playtype hysteresis model posses difficulties for convergence. Similarly in [10], non-vertical scanning curves have been introduced to regularize the sign function for numerical experiments.

Remark 2 *Because of the appearance of the term* $\partial_t u$ *in* (2.2), *the extended playtype hysteresis model requires initial conditions both in pressure and saturation. This is in contrast to the playtype hysteresis where an initial condition in saturation only, is required.*

3 Redistribution

Following Philip [15] , Raats & van Duijn [19] and Pop et al [18] we make the effect of hysteresis explicit in the redistribution case. We show that the extended playtype hysteresis as described by (2.2), with $H(S_w)$ satisfying (2.7) covers all cases of redistribution. This is one of the main purposes of the paper.

3.1 General set up

Consider a horizontal porous column of infinite extent, directed along the x-axis. In the column the flow is one dimensional and describes the redistribution of fluids. We shall restrict ourselves to the case of unsaturated flow, with water as the wetting phase and air as the non-wetting phase. The variables to be determined are the water saturation S_w and pressure u. For brevity we drop the subscript w from the notation. Let $\mathbf{R}^- = \{x < 0\}$ and $\mathbf{R}^+ = \{x > 0\}$ denote respectively the left and right half of the column. The governing equations are Richards equation (1.3) along with closure relation (2.2):

$$\partial_t S + \partial_x F = 0, \text{ for } x \in \mathbf{R}, t > 0, \tag{3.1}$$

$$F = k(S)\partial_x u \quad \text{for } x \in \mathbf{R}, t > 0, \tag{3.2}$$

$$u \in P^+(S) - P^-(S) \cdot \operatorname{sign}(\partial_t H(S) + \partial_t u). \tag{3.3}$$

The halves $\mathbf{R}^-$ and $\mathbf{R}^+$ have constant, but different, initial saturation and pressure at $t = 0$. We impose

$$S(x,0) = \begin{cases} S_l & \text{for } x \in \mathbf{R}^- \\ S_r & \text{for } x \in \mathbf{R}^+; \end{cases} \tag{3.4}$$

and

$$u(x,0) = \begin{cases} u_l & \text{for } x \in \mathbf{R}^-, \\ u_r & \text{for } x \in \mathbf{R}^+. \end{cases} \tag{3.5}$$

Throughout this paper we assume that the functions k, P_{im}, P_{dr} and H are smooth and satisfy the structural properties:

(A. 1) $k(0) = 0$; $k(S)$, $\frac{dk}{dS}(S) > 0$ for $0 < S \leq 1$ with $k(1) < \infty$.

(A. 2) $P_{dr}(S) > P_{im}(S) > 0$ if $0 < S < 1$ with $P_{dr}(1) \geq P_{im}(1) = 0$.

(A. 3) $\frac{dP_{im}}{dS}(S), \frac{dP_{dr}}{dS}(S) < 0$ for $0 < S < 1$.

(A. 4) H satisfies (2.7).

For the initial conditions (3.4) and (3.5) to be consistent with expression (3.3) we must impose,

$$P_{im}(S_i) \leq u_i \leq P_{dr}(S_i) \quad \text{for } i = l, r. \tag{3.6}$$

In this and later sections we use the notation,

Definition 2 *$E_l := (S_l, u_l)$ and $E_r = (S_r, u_r)$.*

Thus in terms of Definitions 1 and 2, condition (3.6) reads: $E_l, E_r \in \mathcal{H} \cup \partial\mathcal{H}^{im} \cup \partial\mathcal{H}^{dr}$. Since $E_l \neq E_r$, a solution of (3.1)-(3.5) is expected to have a discontinuous saturation at $x = 0$. Only in exceptional cases the saturation is continuous across $x = 0$. But mass conservation and momentum conservation requires the flux F and the pressure u to be continuous. Thus the strategy is to solve (3.1)-(3.3) separately for $\mathbf{R}^-$ and for $\mathbf{R}^+$, subject to (3.4) and (3.5) and then to match possible solutions so that flux and pressure are continuous at $x = 0$. Such solutions will be either in the imbibition state or in the drianage state in $\mathbf{R}^-$ and $\mathbf{R}^+$. Thus in addition to (3.1)-(3.5) we shall explicitly use

$$\begin{aligned} u(0^-, t) &= u(0^+, t), \\ F(0^-, t) &= F(0^+, t), \end{aligned} \tag{3.7}$$

for each $t > 0$. Here we use the notation $f(0^{\pm}) = \lim_{x \uparrow\downarrow 0} f(x)$.

3.2 Possible initial conditions

Let $E_r \in \partial\mathcal{H}^{dr}$, $E_l \in \partial\mathcal{H}^{im}$ and let $u_l > u_r$. Since this implies $S_l < S_r$ one expects that water flows from the wet half column to the dry half column. This is called "conventional flow". It is described by Philip in his classical paper [15].

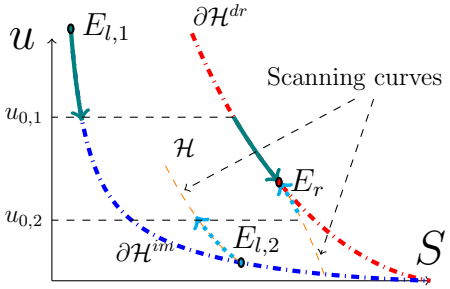

Figure 5: (green) Redistribution according to Philip [15] yielding "conventional" flow; (cyan) redistribution according to Raats & van Duijn yielding "unconventional" flow. The arrows indicate the direction of increasing x.

He found that in this case the right half column ($\mathbf{R}^+$) is in the drainage state, with (S, u) following a trajectory on $\partial\mathcal{H}^{dr}$, and the left half column ($\mathbf{R}^-$) is in the imbibition state, with (S, u) following a trajectory on $\partial\mathcal{H}^{im}$. These trajectories are connected at $x = 0$ by a horizontal jump in the (S, u) plane where $u = u_{0,1} \in (u_r, u_l)$. This value is uniquely chosen so that the flux is continuous. The behavior is sketched in the (S, u) plane in Figure 5.

However it was later realized and pointed out (Raats & van Duijn [19]) that this construction fails for $u_l < u_r$. Then one has to use the scanning curves emerging from the points E_l and E_r as in Figure 5. With these scanning curves one follows the same procedure. But now the left half is in the drainage state and becomes drier, while the right half is in imbibition state and becomes wetter. This is called "unconventional flow" because additionally if $S_l < S_r$ then counterintuitively water flows from the dry half to the wet half. Using the Maulem model, Heinen & Raats [8] demonstrated numerically that this type of redistribution can indeed occur.

Going one step further one can question what happens when $E_i \in \mathcal{H}$ $(i = l, r)$. Although redistribution results arising from interfacial area models [18] are available for general pressure and saturation initial conditions, they do not specify any directions in the induced P_c-S_w curves. Thus they can not describe hysteretic redistribution in the broadest sense. This is the same reason why redistribution results for heterogeneous semi-infinite blocks [23] cannot be extended to cover hysteretic domains.

Remark 3 *In the extended playtype model, the primary scanning curves are described by equation* (2.3)*. On such curves in* $\mathcal{H}$ *one can, in principle, go back and forth: i.e. the same scanning curves are used for drainage and imbibition. Hence no secondary scanning curves are generated. However, this is not an obstacle for horizontal redistribution, as the right/left half of the column can only be in one state: either drainage or imbibition.*

4 Self-Similar solutions

4.1 Preliminaries

Because the initial conditions are piecewise constant, one can reduce the system of partial differential equations (3.1)-(3.5) to a system of ordinary differential equations by introducing the similarity transformation:

$$\begin{cases} S(x,t) = S(\eta), \quad u(x,t) = u(\eta), \quad F(x,t) = F(\eta) \\ \text{where } \eta = \dfrac{x}{\sqrt{t}}, \quad -\infty < \eta < \infty. \end{cases} \tag{4.1}$$

Substituting (4.1) into (3.1)-(3.3) and using initial conditions (3.4)-(3.5) one obtains the boundary value problem $(\mathcal{P})$: (we will use primes to denote differentiation with respect to η)

$$(\mathcal{P}) \begin{cases} \dfrac{\eta}{2} S' = F', \quad F = k(S)u' \quad \text{for } \eta \in \mathbf{R}/\{0\} & (4.2) \\ u \in P^+(S) - P^-(S) \cdot \operatorname{sign}\left[-\eta(H(S)+u)'\right] & (4.3) \\ (S(\eta), u(\eta)) \to E_l \quad \text{as } \eta \to -\infty & (4.4) \\ (S(\eta), u(\eta)) \to E_r \quad \text{as } \eta \to \infty. & (4.5) \end{cases}$$

Here flux F has been redefined: it is $\sqrt{t}$ times the original flux. To obtain (4.3) we used

$$\text{sign}\left[\partial_t(H(S)+u)\right] = \text{sign}\left[-\frac{\eta}{2t}(H(S)+u)'\right] = \text{sign}\left[-\eta(H(S)+u)'\right].$$

In problem $(\mathcal{P})$ the pressure u and the flux F are continuous. Integrating by parts the first equation in (4.2), the flux continuity implies that $\eta S(\eta)$ is continuous as well. Hence the saturation S can only be discontinuous at $\eta = 0$.

When discussing the solutions of Problem $(\mathcal{P})$ we shall represent them as trajectories $\{(S(\eta), u(\eta)) : -\infty < \eta < \infty\}$ in the (S, u) plane. The trajectories run from E_l (as $\eta \to -\infty$) to E_r (as $\eta \to \infty$). In the figures below the arrows indicate the direction of increasing η.

Remark 4 *The smoothness of the coefficients in* (4.2)-(4.5) *implies that the functions* (S, F, u) *are smooth when* $\eta \neq 0$ *and the equations are satisfied classically except at points where* (S, u) *moves from one of the sets* $\mathcal{H}$, $\partial\mathcal{H}^{im}$, $\partial\mathcal{H}^{dr}$ *to another.*

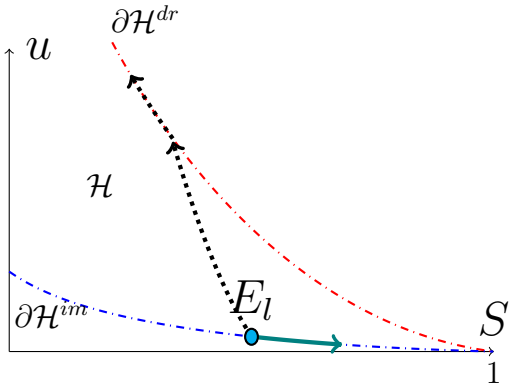

Figure 6: Possible solutions of Problem $(\mathcal{P})$ emerging from $E_l \in \partial\mathcal{H}^{im}$. The arrows indicate increasing η.

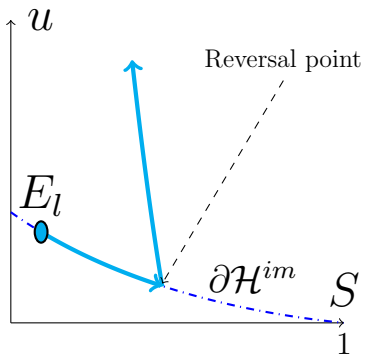

Figure 7: Switch from imbibition to scanning curve.

We first consider all possible solutions in $\mathbf{R}^-$, that satisfy boundary conditions (4.4). We distinguish the following three cases:

Case 1. $E_l \in \partial\mathcal{H}^{im}$ **(i.e.** $u_l = P_{im}(S_l)$**)**

Then there are four possibilities, see Figure 6.

1.1 $(S(\eta), u(\eta)) = E_l$ for all $\eta < 0$;

1.2 $(S(\eta), u(\eta)) \in \partial\mathcal{H}^{im}$ and $S'(\eta) > 0$ for all $\eta < 0$;

1.3 $(S(\eta), u(\eta)) \in \mathcal{H}$ and $S'(\eta) < 0$ for all $\eta < 0$. This implies (see equation (2.3)),

$$H(S(\eta)) + u(\eta) = H(S_l) + u_l \quad \text{for all } \eta < 0;$$

1.4 There exists $\eta_0 < 0$ so that

$$(S(\eta), u(\eta)) \in \mathcal{H} \text{ and } S'(\eta) < 0 \text{ for } -\infty < \eta < \eta_0,$$
$$(S(\eta), u(\eta)) \in \partial\mathcal{H}^{dr} \text{ and } S'(\eta) < 0 \text{ for } \eta_0 \le \eta < 0.$$

One may wonder why in Case 1.2 the trajectory stays on $\partial\mathcal{H}^{im}$ for all $\eta < 0$. Suppose it does not. Then there exists a reversal point $\eta^* < 0$ at which the trajectory switches from the imbibition curve to a scanning curve, as in Figure 7. Since $S'(\eta) > 0$ for $-\infty < \eta < \eta^*$, it follows from (4.2) that $F'(\eta) < 0$ for $-\infty < \eta < \eta^*$. Using $F(-\infty) = 0$, we have $F(\eta^*) < 0$. But this would imply $u'(\eta^*) = \frac{F(\eta^*)}{k(S(\eta^*))} < 0$, contradicting the reversal of direction at η^*.

This argument can be used repeatedly to show that $S'(\eta)$ cannot change its sign in $\mathbf{R}^-$ which eliminates all other possibilities except the ones presented in Case 1.

Case 2. $E_l \in \mathcal{H}$ **(i.e.** $P_{im}(S_l) < u_l < P_{dr}(S_l)$**)**

Now there are three possibilities, see Figure 8.

2.1 $(S(\eta), u(\eta)) = E_l$ for all $\eta < 0$;

2.2 $(S(\eta), u(\eta)) \in \mathcal{H}$ and $S'(\eta) \lneqq 0$ for all $\eta < 0$. Again this implies

$$H(S(\eta)) + u(\eta) = H(S_l) + u_l$$

for all $\eta < 0$;

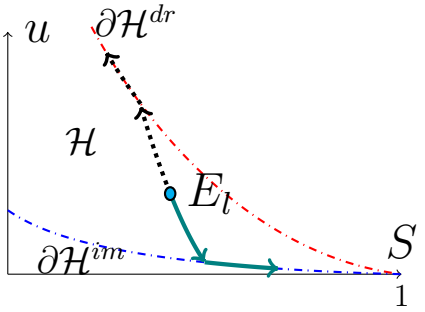

Figure 8: Possible solutions of Problem $(\mathcal{P})$ emerging from $E_l \in \mathcal{H}$.

2.3 There exists $\eta_0 < 0$ so that

$$(S(\eta), u(\eta)) \in \mathcal{H} \text{ for } -\infty < \eta < \eta_0,$$

and either $(S(\eta), u(\eta)) \in \partial\mathcal{H}^{im}$ for $\eta_0 \le \eta < 0$ and $S'(\eta) > 0$ for all $-\infty < \eta < 0$, or $(S(\eta), u(\eta)) \in \partial\mathcal{H}^{dr}$ for $\eta_0 \le \eta < 0$ and $S'(\eta) < 0$ for all $-\infty < \eta < 0$.

Case 3. $E_l \in \partial\mathcal{H}^{dr}$ **(i.e.** $u_l = P_{dr}(S_l)$**)**

As in Case 1 there are four possibilities, see Figure 9.

3.1 $(S(\eta), u(\eta)) = E_l$ for all $\eta < 0$;

3.2 $(S(\eta), u(\eta)) \in \partial\mathcal{H}^{dr}$ and $S'(\eta) < 0$ for all $\eta < 0$;

3.3 $(S(\eta), u(\eta)) \in \mathcal{H}$ and $S'(\eta) > 0$ for all $\eta < 0$, again giving

$$H(S(\eta)) + u(\eta) = H(S_l) + u_l$$

for all $\eta < 0$;

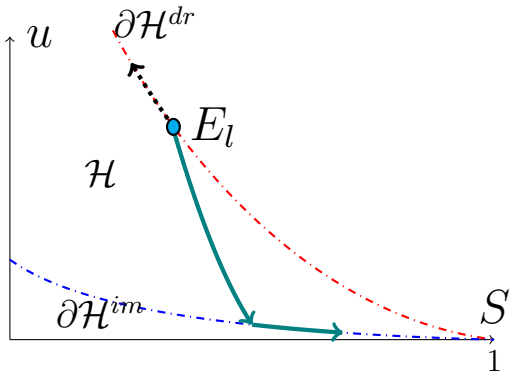

Figure 9: Possible solutions of Problem $(\mathcal{P})$ emerging from $E_l \in \partial\mathcal{H}^{dr}$.

3.4 There exists $\eta_0 < 0$ so that

$$(S(\eta), u(\eta)) \in \mathcal{H} \text{ and } S'(\eta) > 0 \text{ for } -\infty < \eta < \eta_0,$$
$$(S(\eta), u(\eta)) \in \partial\mathcal{H}^{im} \text{ and } S'(\eta) > 0 \text{ for } \eta_0 \le \eta < 0.$$

A similar distinction of possible solutions can be made with respect to E_r. We omit the details. So far we have shown how the piecewise solutions can be in $\mathbf{R}^-$ and $\mathbf{R}^+$. To combine the solutions of two half columns we present one final observation.

Sign of F

Except for the trivial case $S(\eta) = S_l$ for $\eta < 0$ and $S(\eta) = S_r$ for $\eta > 0$ (implying that $F(\eta) = 0$ for all $-\infty < \eta < \infty$) we observe that the sign of $S'(\eta)$ is either strictly positive or strictly negative in the half columns $\mathbf{R}^-$ and $\mathbf{R}^+$. We now show that this implies that the flux F cannot change its sign in the whole column: either $F(\eta) > 0$ or $F(\eta) < 0$ for all $-\infty < \eta < \infty$.

Suppose $S'(\eta) < 0$ for $\eta < 0$. Then (4.2) implies $F'(\eta) > 0$ for $\eta < 0$. Using this and the flux $F(-\infty) = 0$ we find $F(\eta) > 0$ for all $\eta < 0$. In particular, by continuity of the flux, $F(0) > 0$. This observation, the fact that $F'(\eta)$ has a fixed sign for $\eta > 0$ and $F(\infty) = 0$ imply $F(\eta) > 0$ for all $\eta > 0$. A similar argument is used when $S'(\eta) > 0$ for $\eta < 0$. Since $u_r - u_l = \int_{-\infty}^{\infty} u' = \int_{-\infty}^{\infty} \frac{F(\eta)}{k(S(\eta))}$ we conclude

4.1 If $u_r > u_l$ then $F(\eta) > 0$ and $u'(\eta) > 0$ for all $\eta \in \mathbf{R}$.

4.2 If $u_r < u_l$ then $F(\eta) < 0$ and $u'(\eta) < 0$ for all $\eta \in \mathbf{R}$.

The cases discussed above for E_l, and likewise for E_r, are the building blocks in the construction of the full solution. This is discussed in the next subsection.

Remark 5 Redistribution and playtype hysteresis: *With playtype hysteresis the expression* (1.5) *is used. Since no time derivative of pressure is involved, one has for redistribution an initial saturation only given by* (3.4)*. In case of 'unconditional' flow, as suggested in [19], the* (S, u) *profile will lie on scanning curves for* $x \neq 0$ *which means for playtype hysteresis model* S *will be constant for* $x < 0$ *and* $x > 0$*. Using this result in* (3.1) *we get that,* $F(x,t)$ *is constant for all* $x \in \mathbf{R}$ *and* $t > 0$*. Since* $F(\pm\infty, t) = 0$ *(any other value would give a unbounded pressure in* $\pm\infty$ *from* (3.2)*) we have* $F(x,t) = 0$ *for all* $x \in \mathbf{R}$ *and* $t > 0$*, meaning that the pressure* $u = u_0 =$ constant *for all* $x \in \mathbf{R}$*. This observation has the following consequence:*

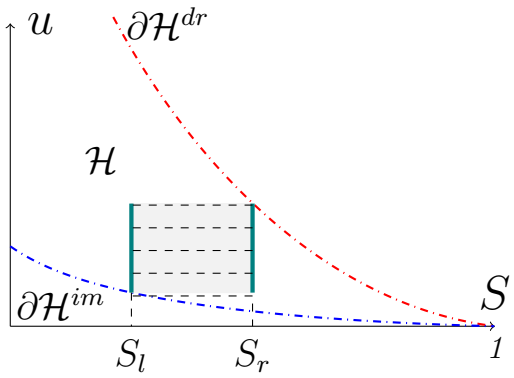

Figure 10: Possible solutions with playtype hysteresis.

If $P_{im}(S_l) \leq P_{dr}(S_r)$*, then any horizontal connection is possible as indicated in Figure 10. The corresponding saturation profile is 'frozen' in the sense that:*

$$S(x,t) = \begin{cases} S_l & \text{for } x < 0 \\ S_r & \text{for } x > 0 \end{cases} \tag{4.6}$$

for all $t > 0$*. And the pressure is a undetermined constant* u_0 *as long as* $P_{im}(S_l) \leq u_0 \leq P_{dr}(S_r)$*. If however* $P_{im}(S_l) \geq P_{dr}(S_r)$ *then the solution is given by classical Philip construction.*

Interestingly, the saturation profile remains frozen even when the domain is finite. If the domain is $[-1, 1]$ *and Neumann conditions* $F(\pm 1, t) = 0$ *(no flow) are imposed at the boundaries for* $t > 0$*, then by the same argument on can get frozen saturations as given in* (4.6)*.*

4.2 Construction for $E_r \in \partial\mathcal{H}^{dr}$, $E_l \in \partial\mathcal{H}^{im}$

We use the building blocks (cases and sub-cases from Section 4.1) to construct the full solution of problem $(\mathcal{P})$ for given E_l and E_r. With reference to Figure 11 we fix a point $E_r \in \partial\mathcal{H}^{dr}$ and let S_* be such that $P_{im}(S_*) = u_r$. Further the curve $H(S)+u = H(S_r)+u_r$ intersects $\partial\mathcal{H}^{im}$ at $S = S^*$. Clearly $0 < S_* < S^* < 1$. Below we consider five typical positions for E_l with respect to the given E_r. It is relatively straightforward to check that the constructions, presented below, are the only ones allowed based on our discussions in Section 4.1.

(i) $0 < S_l < S_*$. This is the classical Philip redistribution. In terms of Section 4.1 we have Case 1.2 for E_l and a similar case for E_r. The exact value of $u = u_{0,1}$ at $\eta = 0$, where the saturation jumps, needs to be determined from the flux continuity.

(ii) $S_l = S_*$. Special case where no flow occurs and the system is in equilibrium. Here the flux $F(\eta) = 0$ for all $\eta \in \mathbf{R}$. It is Case 1.1 for E_l and Case 3.1 for E_r.

(iii) $S_* < S_l < S^*$. This is unconventional flow since the dry (left) half column becomes drier and the wet (right) half column wetter, if $S_l < S_r$. Here $(S(\eta), u(\eta)) \in \mathcal{H}$ for all $\eta \in \mathbf{R}$. It is Case 1.3 for E_l and similar for E_r. As before, the value of $u = u_{0,3}$ at $\eta = 0$ follows from flux continuity.

(iv) $S_l = S^*$. As in (iii), but now $\{(S(\eta), u(\eta)) : \eta \in \mathbf{R}\}$ belongs to a single scanning curve. Here the saturation is continuous at $\eta = 0$.

(v) $S^* < S_l < 1$. This is a rather complicated case. Depending on the position of E_l with respect to E_r three connections (i.e. solutions) are possible. One is shown in Figure 11 where $(S(\eta), u(\eta)) \in \mathcal{H}$ for all $\eta \in \mathbf{R}$. This situation relates to the Case 1.3 for E_l and similar for E_r. But there are also connections possible using part of $\partial\mathcal{H}^{dr}$ (Case 1.4 for E_l) or part of $\partial\mathcal{H}^{im}$ (case similar to 3.4 for E_r). These constructions will be discussed in detail in Section 4.3. The corresponding saturation profiles are sketched in Figure 12.

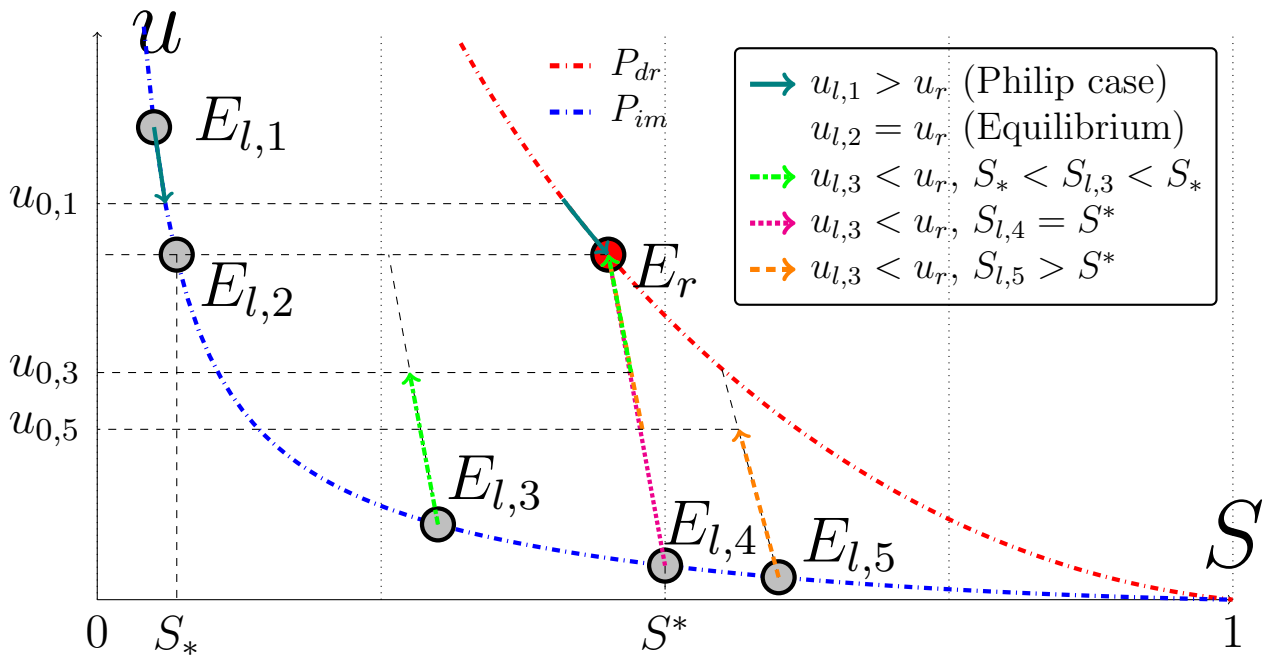

Figure 11: Redistribution scenarios for fixed $E_r \in \partial\mathcal{H}^{dr}$.

In [18] and [23] mathematical aspects of the Philip redistribution (Case (i)) are considered. Before analyzing the other cases in detail, observe that for the extended model

$(S(\eta), u(\eta)) \in \mathcal{H}$ implies that $H(S(\eta))+u(\eta)$ is constant which means that $u' = -\frac{dH}{dS}(S)S'$. Substituting this in (4.2) we get:

$$\frac{\eta}{2}S' + (D_{\mathcal{H}}(S)S')' = 0, \tag{4.7}$$

if $(S(\eta), u(\eta)) \in \mathcal{H}$, where

$$D_{\mathcal{H}} := k(S)\frac{dH}{dS}(S). \tag{4.8}$$

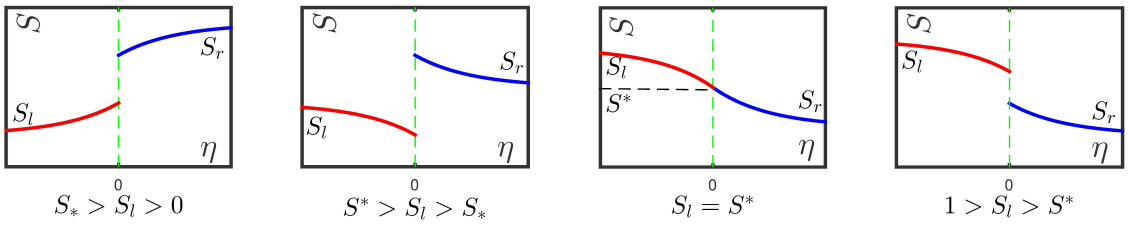

Figure 12: Saturation profiles for $0 < S_l < 1$ when $E_r \in \partial\mathcal{H}^{dr}$ is fixed and $E_l \in \partial\mathcal{H}^{im}$.

Case (iii) and (iv) are covered by (4.7) and (4.8) for $\eta \in \mathbf{R}$, subject to boundary conditions $S(-\infty) = S_l$ and $S(+\infty) = S_r$. Case (iv) is a governed by the general theory in [24] whereas for Case (iii) we need to recall some of the arguments from [18, 23, 24]. To show how to construct the solutions in general, let us briefly consider Case (iii). In this case $(S(\eta), u(\eta)) \in \mathcal{H}$ for $\eta \in \mathbf{R}$ and so for the pressure we have:

$$u = (H(S_l) + u_l) - H(S) \quad \text{in } \mathbf{R}^-, \tag{4.9}$$
$$u = (H(S_r) + u_r) - H(S) \quad \text{in } \mathbf{R}^+. \tag{4.10}$$

Then consider the sub-problems

$$(\mathcal{P}^-)\begin{cases} \frac{\eta}{2}S' + (D_{\mathcal{H}}(S)S')' = 0 \text{ on } \mathbf{R}^-, & (4.11)\\ S(-\infty) = S_l, \quad S(0^-) = S^- < S_l, & (4.12)\\ u \text{ satisfies (4.9)}; & (4.13)\end{cases}$$

and

$$(\mathcal{P}^+)\begin{cases} \frac{\eta}{2}S' + (D_{\mathcal{H}}(S)S')' = 0 \text{ on } \mathbf{R}^+, & (4.14)\\ S(0^+) = S^+ > S_r, \quad S(\infty) = S_r, & (4.15)\\ u \text{ satisfies (4.10)}. & (4.16)\end{cases}$$

In these problems the saturation S^- and S^+ will be chosen so that the pressure u and the flux $F = -D_{\mathcal{H}}(S)S'$ are continuous across $\eta = 0$. From (4.9) and (4.10) it follows that

$$u(0) = H(S_l) + u_l - H(S^-) = H(S_r) + u_r - H(S^+) \tag{4.17}$$

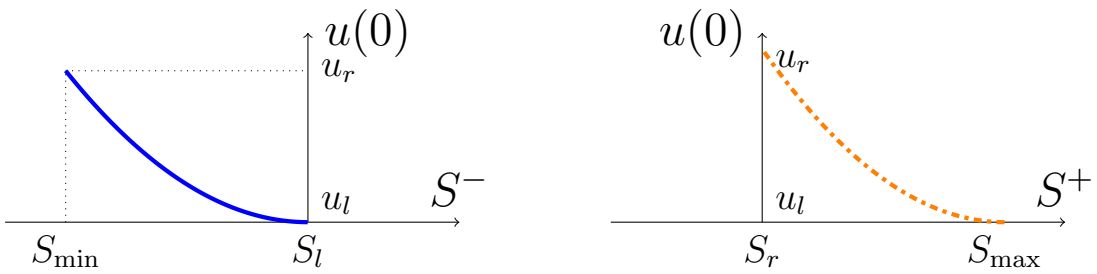

Figure 13: Graphical representation of (4.17). Note that since H satisfies (2.7), $H(S)$ strictly increases with S.

The algebraic conditions imply that if $u(0)$ ranges from u_l to u_r, then S^- ranges from S_l to $S_{\min} < S_l$ and S^+ from $S_{\max} > S_r$ to S_r. Boundary value problems like $(\mathcal{P}^-)$ and $(\mathcal{P}^+)$ have been studied in detail in [24]. There it is shown that the flux at $\eta = 0^\pm$ depends continuously and monotonically on the boundary saturation $S^\pm$. Denoting the flux at $\eta = 0^\pm$ by,

$$F^+(S^+) := F(\eta = 0^+; S^+), \tag{4.18}$$
$$F^-(S^-) := F(\eta = 0^-; S^-), \tag{4.19}$$

then $F^+(S^+)$ is continuous and strictly increasing for $S_r \le S^+ \le S_{\max}$ with $F^+(S_r) = 0$, and $F^-(S^-)$ is continuous and strictly decreasing for $S_{\min} \le S^- \le S_l$ with $F^-(S_l) = 0$. Writing the fluxes as functions of $u(0)$ we have:

- $F^+(u_r) = 0$ and $F^+(u(0))$ is positive, continuous and strictly decreasing for $u_l \le u(0) \le u_r$.
- $F^-(u_l) = 0$ and $F^-(u(0))$ is positive, continuous and strictly increasing for $u_l \le u(0) \le u_r$.

Hence there exists a unique pressure $u(0) = u_0$ where the fluxes intersect, as in Figure 14. This pressure uniquely determines saturations S^+ and S^- by (4.17). Taking the composite function of solutions of $(\mathcal{P}^-)$ and $(\mathcal{P}^+)$ completes the construction of Case (iii).

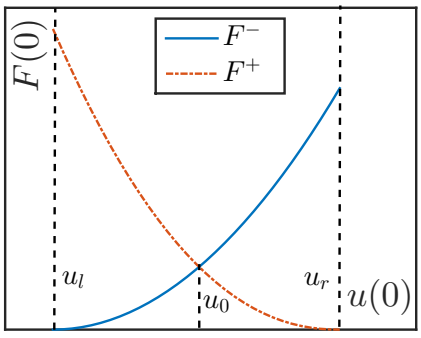

Figure 14: Intersection of fluxes yielding the unique pressure $u(0) = u_0$.

4.3 Construction for arbitrary E_l and E_r

For redistribution positive and negative directions are interchangeable. Therefore without loss of generality we may assume

$$u_l < u_r. \tag{4.20}$$

Again we fix E_r, but this time $E_r \in \mathcal{H} \cup \partial\mathcal{H}^{im} \cup \partial\mathcal{H}^{dr}$. With assumption (4.20) we can sort out all typical cases based on where E_l is located. For this purpose, and with reference to Figure 15, the sets $\mathcal{H}_1$, $\mathcal{H}_2$ and $\mathcal{H}_3$ are introduced. Let S^* and S_* be defined as before and let the curve $H(S) + u = H({P_{dr}}^{-1}(u_r)) + u_r$ intersect $u = P_{im}(S^*)$ at $S = S^\dagger$. The formal definitions are:

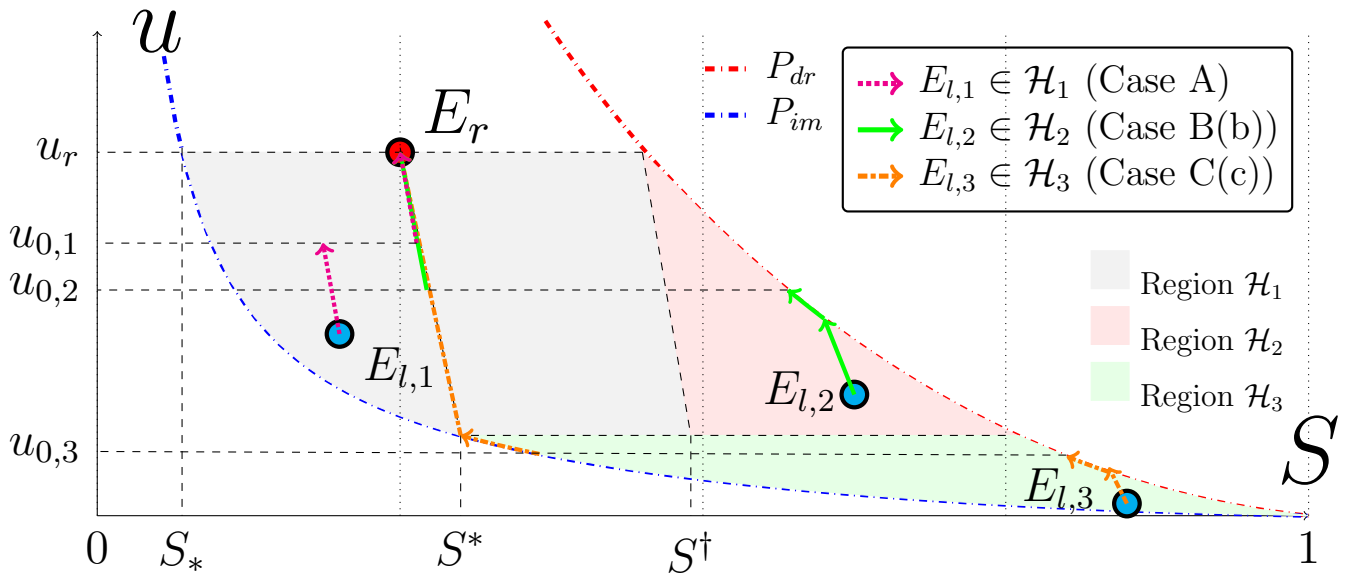

Figure 15: The redistribution scenario for general cases.

Definition 3

$$\mathcal{H}_1 = \{(S,u) : 0 < S < 1, \max\{P_{im}(S), P_{im}(S^*)\} \le u \le \min\{u_r, H({P_{dr}}^{-1}(u_r)) + u_r - H(S)\}\},$$
$$\mathcal{H}_2 = \{(S,u) : 0 < S < 1, \max\{P_{im}(S^*), H({P_{dr}}^{-1}(u_r)) + u_r - H(S)\} \le u \le P_{dr}(S)\},$$
$$\mathcal{H}_3 = \{(S,u) : 0 < S < 1, P_{im}(S) \le u \le \min\{P_{im}(S^*), P_{dr}(S)\}\}.$$

Accordingly we distinguish

4.3.1 Case A: $E_l \in \mathcal{H}_1$

This situation is similar to Case (iii) in Section 4.2. Here $(S(\eta), u(\eta)) \in \mathcal{H}_1 \cap \mathcal{H}$ for all $\eta \in \mathbf{R}$. Hence one uses Problems $(\mathcal{P}^-)$ and $(\mathcal{P}^+)$ to determine the saturations S^- and S^+ and the pressure $u(0)$ for which the flux is continuous at $\eta = 0$. Figure 15 shows the trajectory running from $E_l = E_{l,1}$ to E_r. It is comprised of (part of) the scanning curve through $E_{l,1}$ and (part of) the scanning curve through E_r. At $\eta = 0$ is the horizontal switch where $u(0) = u_{0,1}$.

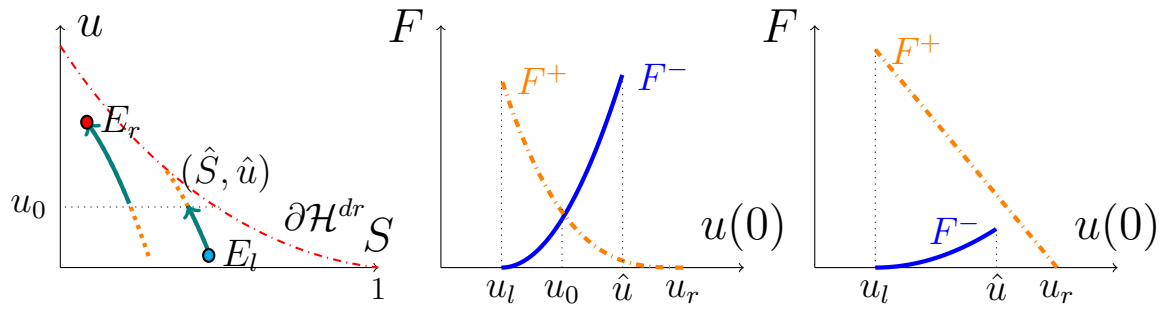

(a) (b) (c)

Figure 16: (a) Possible switch with $u_l < u_0 < \hat{u}$; (b) Intersection of fluxes; (c) no intersection with $F^+(\hat{u}) > F^-(\hat{u})$.

4.3.2 Case B: $E_l \in \mathcal{H}_2$

For left states in this set there are two possibilities. One is as described above for $E_l \in \mathcal{H}_1$, that is $(S(\eta), u(\eta)) \in \mathcal{H}$ for all $\eta \in \mathbf{R}$. We call this possibility 'Case B(a)'. The other possibility is more involved and needs further attention. It occurs when E_l is close to $\partial\mathcal{H}^{dr}$. Let $\hat{S}$ denote the saturation at which the scanning curve through E_l intersects $\partial\mathcal{H}^{dr}$, and let $\hat{u} := P_{dr}(\hat{S})$ be the corresponding pressure. Then for $\hat{S} \le S \le S_l$,

$$u = H(S_l) + u_l - H(S). \tag{4.21}$$

Now suppose, as in Figure 16(a), that there is a switch from the scanning curve through E_l to the scanning curve through E_r. Then (4.9) holds with $\hat{S} < S^- < S_l$ and in terms of the fluxes one would have a unique intersection at $u(0) = u_0$ satisfying $u_l < u_0 < \hat{u}$ (Figure 16(b)). But what if $F^+(\hat{u}) > F^-(\hat{u})$ as in Figure 16(c)? Then the construction fails. We call this case: Case B(b).

To resolve it one needs to follow $u = P_{dr}(S)$ for $S < \hat{S}$. This gives in the left column the pressure saturation relation,

$$u = \begin{cases} H(S_l) + u_l - H(S) & \text{for } \hat{S} < S \le S_l, \\ P_{dr}(S) & \text{for } S \le \hat{S}. \end{cases} \tag{4.22}$$

In the right hand column ($\mathbf{R}^+$) relation (4.10) still holds. This leads to the same problem ($\mathcal{P}^+$) in ($\mathbf{R}^+$), but to a modified problem in $\mathbf{R}^-$:

$$(\hat{\mathcal{P}}^-) \begin{cases} \dfrac{\eta}{2} S' + (\hat{D}(S)S')' = 0 \text{ in } \mathbf{R}^-, \\ S(-\infty) = S_l, \quad S(0^-) = S^- < S_l, \\ u \text{ satisfies (4.22) in } \mathbf{R}^-; \end{cases}$$

where

$$\hat{D}(S) = \begin{cases} k(S)\dfrac{dH}{dS}(S) & \text{for } \hat{S} < S \leq S_l \\ -k(S)\dfrac{dP_{dr}}{dS}(S) & \text{for } S \leq \hat{S} \end{cases}.$$

Here the diffusivity $\hat{D}$ is (in general) discontinuous at $\hat{S}$. But the results in [24] only require boundedness of the diffusivity. Thus with the notation of Section 4.2 (where we use $\hat{F}^-$ to denote the flux in problem $(\hat{\mathcal{P}}^-)$), we have that $\hat{F}^-(S^-)$ is strictly decreasing and continuous for $S^- < S_l$ with $\hat{F}^-(S_l) = 0$. In terms of the pressure $u(0)$, the flux is strictly increasing and continuous for $u_l \leq u(0) \leq u_r$ with $\hat{F}^-(u_l) = 0$. Thus, as in Figure 17, the fluxes $\hat{F}^-$ and F^+ intersect at a unique pressure $u(0) = u_0$. The composite function of the solution of $(\hat{\mathcal{P}}^-)$ and $(\mathcal{P}^+)$ describe the case of redistribution.

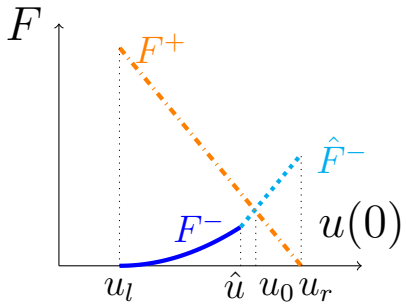

Figure 17: Intersection of the fluxes with $\hat{F}^-$ and F^+

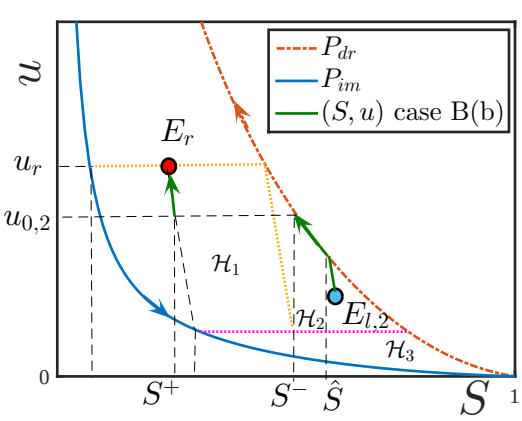

(a) (S, u) trajectories for case B(b)

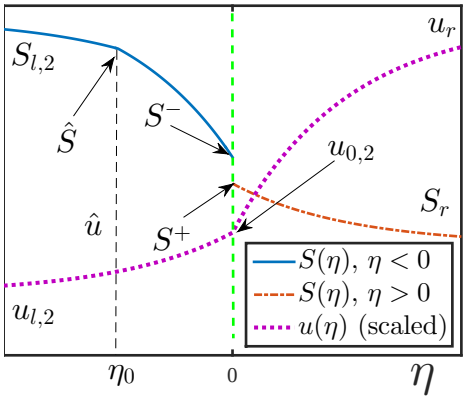

(b) u and S vs. η for case B(b)

Figure 18: Behaviour of saturation S and pressure u between $E_{l,2}$ and E_r.

Figure 18(a) shows the trajectory running from $E_l = E_{l,2}$ to E_r. It is composed of (part of) the scanning curve through $E_{l,2}$, part of $\partial\mathcal{H}^{dr}$ and then (part of) scanning curve through E_r. The horizontal segment or switch is at $\eta = 0$ when $u(0) = u_{0,2}$. The corresponding saturation and pressure are sketched in Figure 18(b) as functions of η. Due to the discontinuity in $\hat{D}(S)$ at $S = \hat{S}$, the saturation has a kink at $S = \hat{S}$ corresponding to $\eta = \eta_0$ (η_0 is defined in Case 2.3, Section 4.1). The pressure has a kink at $\eta = 0$ due to the jump in saturation.

4.3.3 Case C: $E_l \in \mathcal{H}_3$

There are two arrangements, denoted by Case C(a) and Case C(b), that are similar to the Cases B(a) and B(b) respectively. But in this set one has $u_l < P_{im}(S^*)$, implying that a third type of construction is possible where (part of) the two scanning curves, $\partial\mathcal{H}^{dr}$ as well as $\partial\mathcal{H}^{im}$ are being used. We call this 'Case C(c)'.

Let $u^* := P_{im}(S^*)$. Case C(c) arises if

$$F^+(u = u^*) < \hat{F}^-(u = u^*), \tag{4.23}$$

where the fluxes F^+ and $\hat{F}^-$ are defined in the description of previous cases. If (4.23) holds, then the fluxes cannot intersect when $u^* < u(0) < u_r$, see Figure 19. To resolve this situation one needs to modify Problem $(\mathcal{P}^+)$ by including P_{im}, similar to the definition of Problem $(\hat{\mathcal{P}}^-)$. The remaining argument is omitted since it is almost identical to the argument used for $E_l \in \mathcal{H}_2$. Figure 15 shows the trajectory running from $E_l = E_{l,3}$ to E_r.

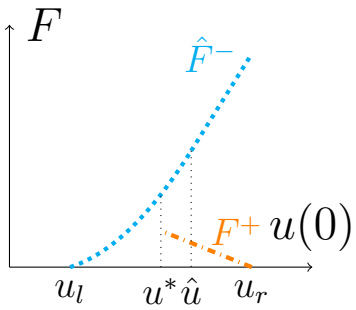

Figure 19: Non-intersection of the fluxes when $E_l \in \mathcal{H}_3$.

5 Numerical study

In this section we present a numerical approach for the redistribution problem and use our theoretical findings to classify and validate the computational results.
For sufficiently large (dimensionless) $W > 0$ we consider the initial-boundary value problem (compare (3.1)-(3.5))

$$\partial_t S + \partial_x F = 0 \text{ for } |x| < W, t > 0, \tag{5.1}$$
$$F = k(S)\partial_x u \quad \text{for } |x| < W, t > 0, \tag{5.2}$$
$$u \in P^+(S) - P^-(S) \cdot \operatorname{sign}(\partial_t H(S) + \partial_t u); \tag{5.3}$$

with

$$S(x,0) = \begin{cases} S_l & \text{for } -W < x < 0, \\ S_r & \text{for } 0 < x < W, \end{cases} \tag{5.4}$$

$$u(x,0) = \begin{cases} u_l & \text{for } -W < x < 0, \\ u_r & \text{for } 0 < x < W, \end{cases} \tag{5.5}$$

and

$$F(\pm W, t) = 0 \text{ for } t > 0. \tag{5.6}$$

For sufficiently small time t, the zero-flux boundary conditions (5.6) have a negligible influence on the redistribution process. Hence, for small t, a solution of (5.1)-(5.6) behaves as if the domain is unbounded and is close to the self-similar solutions discussed in this paper. We will reveal all typical cases.

5.1 Numerical scheme

First thing is to replace the sign$(\cdot)$ graph in (5.3) by a strictly increasing smooth function $\mathcal{G}_\varepsilon$ satisfying:

- $\frac{d\mathcal{G}_\varepsilon}{d\zeta} > 0$ in $\mathbf{R}$ such that $\frac{d\mathcal{G}_\varepsilon}{d\zeta}(0) = \frac{1}{\varepsilon}$ and $\lim_{\varepsilon\to 0} \mathcal{G}_\varepsilon(\zeta) = \text{sign}(\zeta)$ for $\zeta \neq 0$.
- $\lim_{\zeta\to\pm\infty} \frac{d\mathcal{G}_\varepsilon}{d\zeta}(\zeta) = \gamma\varepsilon$ for some constant $\gamma > 0$ and for each $\varepsilon > 0$.

These properties allow us to define the inverse $\Phi_\varepsilon = \mathcal{G}_\varepsilon^{-1}$, so that (5.3) can be written as:

$$\partial_t H(S) + \partial_t u = \Phi_\varepsilon\left(\frac{P^+(S) - u}{P^-(S)}\right). \tag{5.7}$$

Next we introduce the variable:

$$v := H(S) + u, \text{ with } S = H^{-1}(v - u), \tag{5.8}$$

and the function

$$\Psi_\varepsilon(u, v) := \Phi_\varepsilon\left(\frac{P^+(H^{-1}(v-u)) - u}{P^-(H^{-1}(v-u))}\right). \tag{5.9}$$

In terms of u, v and Ψ_ε, equations (5.1)-(5.3) are transformed into

$$\partial_t u = \frac{dH}{dS}(H^{-1}(v-u))\partial_x\left(k(H^{-1}(v-u))\partial_x u\right) + \Psi_\varepsilon(u, v), \tag{5.10}$$

$$\partial_t v = \Psi_\varepsilon(u, v), \tag{5.11}$$

for $|x| < W$ and $t > 0$. Hence we have written (5.1)-(5.3) as a coupled system consisting of a parabolic equation for the pressure u and an ordinary differential equation for v. This type of splitting is well-known in the mathematical literature, for instance see [22].

Let the time interval $[0, T]$ be divided into N intervals of width Δt ($T = N\Delta t$) and let w_n be the variable w at $t = n\Delta t$, with $1 \leq n \leq N$. We calculate v_n from the explicit time-discrete form of (5.11) ($v_0(x) = v(x, 0) = H(S(x, 0)) + u(x, 0)$):

$$v_n = v_{n-1} + \Delta t\Psi_\varepsilon(u_{n-1}, v_{n-1}), \quad \text{for } 1 \leq n \leq N. \tag{5.12}$$

We want to solve (5.10) implicitly for stability. For this, the equation (5.10) needs to be linearized. We use a L-scheme [17] type linearization technique along with inner iterations to solve for u_n. This scheme is defined by (for $i = 1, 2, ...$)

$$\begin{aligned}&(1+L)u_n^i - \Delta t \frac{dH}{dS}(H^{-1}(v_n - u_n^{i-1}))\partial_x \left(k(H^{-1}(v_n - u_n^{i-1}))\partial_x u_n^i\right)\\ &= Lu_n^{i-1} + \Delta t \Psi_\varepsilon(u_n^{i-1}, v_n) + u_{n-1},\end{aligned} \tag{5.13}$$

with $u_n^0 = u_{n-1}$. Here u_n^i is the i^{th} iteration of the n^{th} time step. If assumptions (A.1)-(A.4) are satisfied and if $\partial_x u$, $\partial_u \Psi_\varepsilon$ and $\partial_v \Psi_\varepsilon$ are bounded, then the scheme converges for L sufficiently large and for Δt sufficiently small [17]. In (5.13) we use finite differences for spatial discretization and the whole scheme was implemented in Matlab. In the computations we use

$$W = 100, \quad \Delta x = 0.1, \quad \Delta t = 0.001 \text{ and } L = 1.$$

5.2 Numerical results

The numerical results are obtained for

$$k(S) = S^2 \text{ and (for simplicity) } H(S) = \frac{S}{\delta} \text{ with } \delta = \frac{1}{40}.$$

For P_{dr} and P_{im} we took somewhat artificial expressions in order to visualize all possible cases:

$$P_{im}(S) = \frac{1}{5}\left(\frac{1}{S} - 1\right) + \frac{2}{5}(1-S)^2 \quad \text{and} \quad P_{dr}(S) = \left(\frac{1}{S} - 1\right) + 6(1-S)^2.$$

Taking realistic (van Genuchten) expressions would make some of the cases hard to distinguish. Finally we use for Φ_ε the expression

$$\Phi_\varepsilon(\zeta) = \begin{cases} \sqrt[3]{\frac{\varepsilon}{\gamma}} + \frac{1}{\gamma\varepsilon}(\zeta - 1) & \text{for } \zeta > 1 \\ \dfrac{\varepsilon\zeta}{\sqrt{1 - (1 - (\varepsilon^2\gamma)^{\frac{2}{3}})\zeta^2}} & \text{for } \zeta \in [-1, 1] \\ -\sqrt[3]{\frac{\varepsilon}{\gamma}} + \frac{1}{\gamma\varepsilon}(\zeta + 1) & \text{for } \zeta < -1 \end{cases},$$

where $\varepsilon = 10^{-4}$ (fixed). Observe that Φ_e is continuously differentiable in $\mathbf{R}$. The value of γ can be chosen small as long as $(S, u) \in \mathcal{H}$ (then $\gamma = 1$), but needs a large value when (S, u) is on $\partial\mathcal{H}^{im}$ or on $\partial\mathcal{H}^{dr}$.

Given the size of the domain ($W = 100$) we would show the computational results at $t = 1$. This is sufficiently small so that the zero-flux boundary conditions have no influence

on the redistribution process. We visualize the results as trajectories in the (S, u) plane (i.e. $(S(x,t), u(x,t))$ where x runs from $-W$ to W) and as profiles of $x = \eta = \frac{x}{\sqrt{t=1}}$.

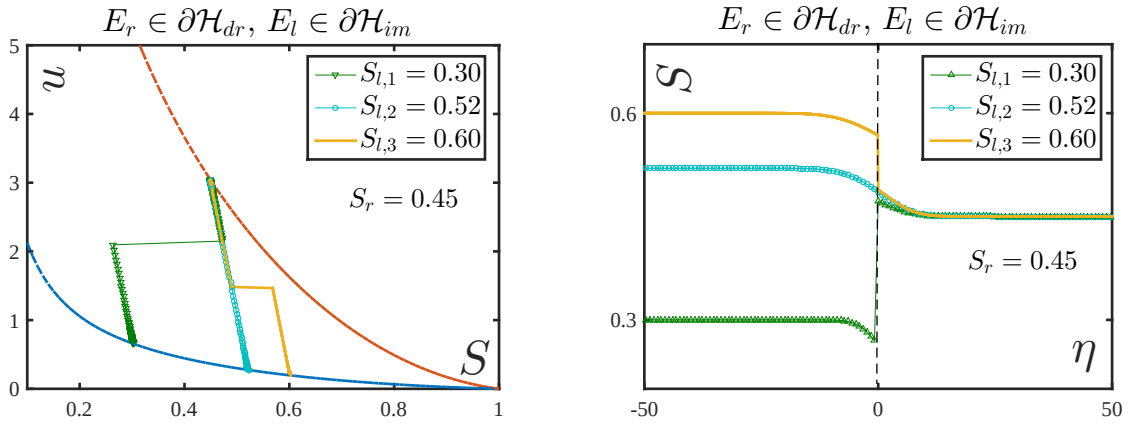

(a) (S, u) profiles (b) S vs. η profiles

Figure 20: Numerical results for $E_r \in \partial\mathcal{H}^{dr}$ fixed and $E_l \in \partial\mathcal{H}^{im}$ variable, at $t = 1$. Here $S_r = 0.45$ and $S_{l,1} = 0.30$ (unconventional flow); $S_{l,2} = 0.52 = S^*$ (saturation is continuous) and $S_{l,3} = 0.60$ (conventional flow corresponding to Case C(a)).

Figure 20 shows results where $E_r \in \partial\mathcal{H}^{dr}$ is fixed and where $E_l \in \partial\mathcal{H}^{im}$ is varied. Note that the green trajectory represents unconventional flow because the trajectory moves to the left when leaving E_l and when entering E_r. This means that the dry half column becomes drier and the wet half column becomes wetter.

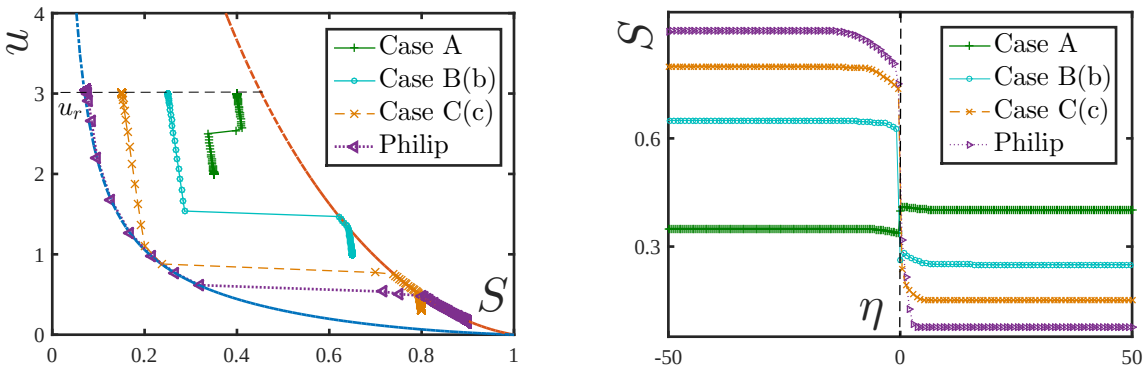

(a) (S, u) profiles (b) S vs. η profiles

Figure 21: Numerical results for $E_l, E_r \in \mathcal{H} \cup \partial\mathcal{H}^{im} \cup \partial\mathcal{H}^{dr}$, where $u_r = 3$ is fixed. With reference to Section 4 we have Case A: $S_r = 0.4$, $E_l = (0.35, 2)$; Case B(b): $S_r = 0.25$, $E_l = (0.65, 1)$; Case C(c): $S_r = 0.15$, $E_l = (0.8, 0.3)$; Philip: $S_r = 0.075$, $E_l = (0.9, 0.17)$.

Figure 21 shows results for $E_l, E_r \in \mathcal{H} \cup \partial\mathcal{H}^{im} \cup \partial\mathcal{H}^{dr}$. Here we took $\gamma = 100$ to get convergence of the iterations in (5.13). The cases discussed in Section 4 are accurately recovered by the computations. This validates the analysis and explains the complex behaviour of the computed saturation and pressure. The agreement is excellent.

6 Conclusion

In this paper we discussed different hysteresis models for multiphase flow through porous media. To incorporate the effect of non-vertical scanning curves in a simple closed form, we proposed an extension to the playtype hysteresis model and showed that this model resembles the experimental scanning curves accurately. We outlined different properties of the model and discussed available physical and numerical justifications for the model.

After this we investigated horizontal redistribution in an infinite coloumn in the context of hysteresis. In this problem, the two halves of the infinite horizontal porous column have different but constant initial saturation and pressure conditions that causes redistribution to occur. It was pointed out that existing models cannot give a complete description of the redistribution phenomenon. The extended hysteresis model was used to analyze the problem and the resulting system of equations was simplified using a similarity transformation. By distinguishing all possible cases and then using the flux and pressure continuity criterion repeatedly, we constructed unique solutions for the redistribution problem. In fact, we showed that redistribution will always take place, even for unconventional cases, if the initial pressure condition is different in the two halves. Moreover, we categorized all possible scenarios of redistribution into different cases.

Finally, a numerical scheme was proposed for the regularized non-linear system of equations arising from the extended model that converges irrespective of initial guesses. Numerical results from the scheme corroborated with our analytical findings.

Acknowledgment

The first author acknowledges the support of the Darcy Centre of Utrecht University and Eindhoven University of Technology. The second author is supported by Shell and the Netherlands Organisation for Scientific Research (NWO) through the CSER programme (project 14CSER016) and by the Hasselt University through the project BOF17BL04. Both authors thank Prof. I.S. Pop (Hasselt University, University of Bergen) for many fruitful discussions on the subject.

References

[1] J. Bear. *Dynamics of flow in porous media.* 1972.

[2] A.Y. Beliaev and S.M. Hassanizadeh. A theoretical model of hysteresis and dynamic effects in the capillary relation for two-phase flow in porous media. *Transport in Porous Media*, 43(3):487–510, 2001.

[3] M. Brokate, N.D. Botkin, and O.A. Pykhteev. Numerical simulation for a two-phase porous medium flow problem with rate independent hysteresis. *Physica B: Condensed Matter*, 407(9):1336–1339, 2012.

[4] R.H. Brooks and A.T. Corey. Properties of porous media affecting fluid flow. *Journal of the Irrigation and Drainage Division*, 92(2):61–90, 1966.

[5] R.E. Collins. *Flow of fluids through porous materials.* Petroleum Publishing Co.,Tulsa, OK, Jan 1976.

[6] S.M. Hassanizadeh and W.G. Gray. Mechanics and thermodynamics of multiphase flow in porous media including interphase boundaries. *Advances in Water Resources*, 13(4):169 – 186, 1990.

[7] S.M. Hassanizadeh and W.G. Gray. Toward an improved description of the physics of two-phase flow. *Advances in Water Resources*, 16(1):53–67, 1993.

[8] M. Heinen and P.A.C. Raats. Unconventional flow of water from dry to wet caused by hysteresis: A numerical experiment. *Water Resources Research*, 35(8):2587–2590, 1999.

[9] R. Helmig. *Multiphase flow and transport processes in the subsurface: a contribution to the modeling of hydrosystems.* Springer-Verlag, 1997.

[10] A. Lamacz, A. Rätz, and B. Schweizer. A well-posed hysteresis model for flows in porous media and applications to fingering effects. 2010.

[11] N.R. Morrow and C.C. Harris. Capillary equilibrium in porous materials. *Society of Petroleum Engineers*, 1965.

[12] Y. Mualem. A conceptual model of hysteresis. *Water Resources Research*, 10(3):514–520, 1974.

[13] J. Niessner and S.M. Hassanizadeh. A model for two-phase flow in porous media including fluid-fluid interfacial area. *Water Resources Research*, 44(8), 2008.

[14] J.C. Parker, R.J. Lenhard, and T. Kuppusamy. A parametric model for constitutive properties governing multiphase flow in porous media. *Water Resources Research*, 23(4):618–624, 1987.

[15] J. R. Philip. Horizontal redistribution with capillary hysteresis. *Water Resources Research*, 27:1459–1469, 1991.

[16] J.R. Philip. Similarity hypothesis for capillary hysteresis in porous materials. *Journal of Geophysical Research*, 69(8):1553–1562, 1964.

[17] I. S. Pop, F. Radu, and P. Knabner. Mixed finite elements for the richards equation: linearization procedure. *Journal of computational and applied mathematics*, 168(1):365–373, 2004.

[18] I.S. Pop, C.J. van Duijn, J. Niessner, and S.M. Hassanizadeh. Horizontal redistribution of fluids in a porous medium: The role of interfacial area in modeling hysteresis. *Advances in Water Resources*, 32(3):383–390, 2009.

[19] P. A. C. Raats and C. J. van Duijn. A note on horizontal redistribution with capillary hysteresis. *Water Resources Research*, 31(1):231–232, 1995.

[20] L. A. Richards. Capillary conduction of liquids through porous mediums. *Journal of Applied Physics*, 1(5):318–333, 1931.

[21] B. Schweizer. Laws for the capillary pressure in a deterministic model for fronts in porous media. *SIAM Journal on Mathematical Analysis*, 36(5):1489–1521, 2005.

[22] B. Schweizer. The richards equation with hysteresis and degenerate capillary pressure. *Journal of Differential Equations*, 252(10):5594 – 5612, 2012.

[23] C.J. van Duijn and M.J. de Neef. Similarity solution for capillary redistribution of two phases in a porous medium with a single discontinuity. *Advances in Water Resources*, 21(6):451 – 461, 1998.

[24] C.J. van Duijn and L.A. Peletier. A class of similarity solutions of the nonlinear diffusion equation. *Nonlinear Analysis: Theory, Methods & Applications*, 1(3):223 – 233, 1977.

[25] M.T. Van Genuchten. A closed-form equation for predicting the hydraulic conductivity of unsaturated soils. *Soil science society of America journal*, 44(5):892–898, 1980.

[26] A. Visintin. *Differential models of hysteresis*. Springer Science & Business Media, 2013.

[27] L Zhuang. *Advanced theories of water redistribution and infiltration in porous media: Experimental studies and modeling*. PhD thesis, University of Utrecht, Dept. of Earth Sciences, 2017.

UHasselt Computational Mathematics Preprint Series

2017

UP-17-04 *Jonas Zeifang, Klaus Kaiser, Andrea Beck, Jochen Schütz and Claus-Dieter Munz*, **Efficient high-order discontinuous Galerkin computations of low Mach number flows**, 2017

UP-17-03 *M.M. Bosschaert, S.G. Janssens, and Yu.A. Kuznetsov*, **Switching to nonhyperbolic cycles from codim-2 bifurcations of equilibria in DDEs**, 2017

UP-17-02 *Jochen Schütz, David C. Seal and Alexander Jaust*, **Implicit multiderivative collocation solvers for linear partial differential equations with discontinuous Galerkin spatial discretizations**, 2017

UP-17-01 *Alexander Jaust and Jochen Schütz*, **General linear methods for time-dependent PDEs**, 2017

2016

UP-16-06 *Klaus Kaiser and Jochen Schütz*, **A high-order method for weakly compressible flows**, 2016

UP-16-05 *Stefan Karpinski, Iuliu Sorin Pop, Florin A. Radu*, **A hierarchical scale separation approach for the hybridized discontinuous Galerkin method**, 2016

UP-16-04 *Florin A. Radu, Kundan Kumar, Jan Martin Nordbotten, Iuliu Sorin Pop*, **Analysis of a linearization scheme for an interior penalty discontinuous Galerkin method for two phase flow in porous media with dynamic capillarity effects** , 2016

UP-16-03 *Sergey Alyaev, Eirik Keilegavlen, Jan Martin Nordbotten, Iuliu Sorin Pop*, **Fractal structures in freezing brine**, 2016

UP-16-02 *Klaus Kaiser, Jochen Schütz, Ruth Schöbel and Sebastian Noelle*, **A new stable splitting for the isentropic Euler equations**, 2016

UP-16-01 *Jochen Schütz and Vadym Aizinger*, **A hierarchical scale separation approach for the hybridized discontinuous Galerkin method**, 2016